JOURNAL OF GEOPHYSICAL RESEARCH: ATMOSPHERES, VOL. 118, 2809–2820, doi:10.1002/jgrd.50189, 2013

Nitrous oxide (N_2O) emissions from California based on 2010 CalNex airborne measurements

Bin Xiang,[1] Scot M. Miller,[1] Eric A. Kort,[2] Gregory W. Santoni,[1] Bruce C. Daube,[1] Roisin Commane,[1] Wayne M. Angevine,[3] Tom B. Ryerson,[3] Michael K. Trainer,[3] Arlyn E. Andrews,[3] Thomas Nehrkorn,[4] Hanqin Tian,[5] and Steven C. Wofsy[1]

Received 5 June 2012; revised 5 January 2013; accepted 9 January 2013; published 11 April 2013.

[1] Nitrous oxide (N_2O) is an important gas for climate and for stratospheric chemistry, with a lifetime exceeding 100 years. Global concentrations have increased steadily since the 18th century, apparently due to human-associated emissions, principally from the application of nitrogen fertilizers. However, quantitative studies of agricultural emissions at large spatial scales are lacking, inhibited by the difficulty of measuring small enhancements in atmospheric concentration. Here we derive regional emission rates for N_2O in the agricultural heartland of California based on analysis of *in-situ* airborne atmospheric observations collected using a new quantum cascade laser spectrometer. The data were obtained on board the NOAA WP-3 research aircraft during the CalNex (California Research at the Nexus of Air Quality and Climate Change) program in late spring 2010. We coupled the WRF (weather research and forecasting) model, a meso-scale meteorology model, with the STILT (stochastic time-inverted Lagrangian transport) model, a Lagrangian particle dispersion model, to link our *in-situ* airborne observations to surface emissions. We then used a variety of statistical methods to identify source areas and to optimize emission rates. Our results are consistent with the view that fertilizer application is the largest source of N_2O in the Central Valley. The spatial distribution of surface emissions, based on California land use and activity maps, was very different than indicated in the leading emission inventory (EDGAR 4.0). Our estimated total emission flux of N_2O for California in May and June was 3 – 4 times larger than the annual mean given for the state by EDGAR and other inventories, indicating a strong seasonal variation. We estimated the statewide total annual emissions of N_2O to be 0.042 ± 0.011 Tg N/year, roughly equivalent to inventory values if we account for seasonal variations using observations obtained in the midwestern United States. This state total N_2O emission is 20.5 Tg CO_2 equivalent (100 year global warming potential = 310 CO_2 eq/g N_2O), accounting for approximately 4% of the state total greenhouse gas emissions.

Citation: Xiang, B., et al. (2013), Nitrous oxide (N_2O) emissions from California based on 2010 CalNex airborne measurements, *J. Geophys. Res. Atmos.*, *118*, 2809–2820, doi:10.1002/jgrd.50189.

1. Introduction

[2] Atmospheric nitrous oxide (N_2O) is the third most important long-lived anthropogenic greenhouse gas (GHG) and a major component of stratospheric chemical cycles [*Ravishankara et al.*, 2009]. Global atmospheric concentrations of N_2O have increased from a preindustrial value of 275 ppb (nmol/mol) to ~325 ppb presently and continue to increase by 0.2–0.3%/year [*Denman et al.*, 2007]. Total annual global N_2O emissions are calculated to be 18.8 Tg N/year in 2006 [*Syakila and Kroeze*, 2011] based on observed rates of increase and computed loss rates in the stratosphere. About 60% of emissions are from natural processes (e.g., microbial nitrification and denitrification of natural soils and coastal ocean upwelling), and the remaining 40% come from processes associated with human activity, including energy production, industry, biomass burning, direct agricultural emissions from fertilized soils and animal

[1]School of Engineering and Applied Science and Department of Earth and Planetary Sciences, Harvard University, Cambridge, Massachusetts, USA.
[2]Jet Propulsion Laboratory, California Institute of Technology, Pasadena, California, USA.
[3]National Oceanic and Atmospheric Administration, Boulder, Colorado, USA.
[4]Atmospheric and Environmental Research, Lexington, Massachusetts, USA.
[5]School of Forestry and Wildlife Science, Auburn University, Auburn, Alabama, USA.

Corresponding author: Dr. Bin Xiang, School of Engineering and Applied Science, Harvard University, 20 Oxford St., Cambridge, MA 02138, USA. (bxiang@seas.harvard.edu)

2169-897X/13/10.1002/jgrd.50189

manure, and indirect agricultural emissions from nitrogen use (such as atmospheric deposition, leaching and runoff, and human sewage). Agricultural activities are believed to be the main cause of the atmospheric N_2O increase. Anthropogenic N_2O emissions will likely rise in the future, owing to the need to increase agricultural production to accommodate the future population.

[3] Development of effective N_2O regulation strategies must be based on accurate emission estimates at regional and global scales. Current bottom-up estimates of global agricultural N_2O emissions are uncertain, ranging from 4.3 to 5.8 Tg N/year [*Crutzen et al*., 2007; *Davidson*, 2009; *Syakila and Kroeze*, 2011]. This uncertainty mostly arises from deficiencies in constraints on the specific emission factors that are applied to large-scale human activities [*Montzka et al*., 2011]. For "top-down" approaches based on atmospheric observations, data scarcity and transport model inaccuracies are the primary limiting factors. Because of the long lifetime of N_2O (~122 years) [*Volk et al*., 1997] and its diffuse spatial distribution of sources, regional enhancements of N_2O associated with agricultural sources are only ~1% of background concentrations. The relatively small signal enhancements and low signal-to-noise ratio add to the uncertainties in top-down assessments of N_2O emissions.

[4] The Central Valley of California is one of the most productive regions of industrialized agriculture on Earth. Synthetic and organic fertilizer application, animal manure management, wastewater treatment, and crop residual management may all contribute substantially to anthropogenic N_2O emissions in this area. The California Global Warming Solutions Act (Assembly Bill 32, 2006) requires the state to cap its GHG emissions at 1990 levels by year 2020, and the Legislature instructed the California Energy Commission and the Air Resources Board to update the state's GHG inventories every 5 years. Few N_2O measurements have been available for emission inventory validations in California. *Wunch et al*. [2009] studied atmospheric column concentration of N_2O over the South Coast Air Basin and found larger emissions from urban Los Angeles than the EDGAR and California GHG Inventories. Data from a tower in Walnut Grove, California, during April 2010 indicated N_2O emissions in adjacent areas of central California that were roughly three times those estimated by the EDGAR inventories [*Jeong et al*., 2012].

[5] We report here intensive N_2O measurements during the 2010 California Research at the Nexus of Air Quality and Climate Change Campaign (CalNex). These data provide a unique opportunity to assess regional N_2O emissions using the top-down approach. The National Oceanic and Atmospheric Administration (NOAA) WP-3 research aircraft (hereafter referred to as P-3) extensively sampled the atmosphere above the Central Valley in May and June and surveyed Los Angeles and other California cities. The Harvard/Aerodyne Dual Quantum Cascade Laser Spectrometer (QCLS-DUAL, owned by the National Center for Atmospheric Research) was deployed on the P-3. It measured real-time 1 Hz atmospheric N_2O concentrations with 1 s precision of 0.09 ppb and 0.3 ppb accuracy [*Jimenez et al*., 2005; *Kort et al*., 2011]. CalNex represents the first time an airborne sensor of this capability has been deployed for measurements in a major agricultural region.

[6] The top-down approach presented here utilizes observations from the research flights that sampled most intensively over the Central Valley in May and June 2010 coupled with atmospheric model simulations to obtain emission strengths, spatial distributions of sources, and temporal variations over the CalNex period.

2. CalNex Observations

[7] CalNex airborne measurements provided comprehensive sampling of a wide variety of N_2O sources in California. Six flights successfully covered rice paddies, croplands, and dairy farms in the Central Valley, one each focusing on the northern (Sacramento Valley), middle (Northern San Joaquin Valley), and southern (Southern San Joaquin Valley) parts of the Central Valley separately, in May and again in June 2010. Other CalNex flights sampled in and around the South Coast Air Basin, a densely populated urban region including Los Angeles and surrounding suburbs. The present study addresses N_2O sources in natural and agricultural lands. Hence, the Los Angeles flights are not simulated here, but we do represent in our source models urban emissions that can be advected to the Central Valley.

[8] Figure 1 shows flight tracks and N_2O observations from the six Central Valley agricultural flights, projected onto the California county map. Those flights occurred in late spring and early summer, the critical time period of N_2O emissions for the year [*Miller et al*., 2012], associated with peak rates for soil microbial metabolism. The activities of nitrifying and denitrifying microorganisms are expected to peak during the CalNex period because of increasing soil temperature, application of fertilizer to young crops, tillage of the soil, and irrigation [*Szukics et al*., 2010]. The P-3 cruised over the Central Valley in a reversing rectangular ("boustrophedonic") pattern, flying mostly within the boundary layer (below 500 m) to capture local emission sources and occasionally ascending to the free troposphere to measure the background concentrations in the region. Significant enhancements in N_2O concentrations were commonly observed. In many places, N_2O concentrations correlated with concentrations of CH_4, CO, and CO_2, although the enhancement ratios were variable, highlighting the heterogeneity in N_2O sources. A few locations had increases as high as 3 ppb, as on June 18 when the P-3 flew over the dairy farming region in the Northern San Joaquin Valley. All these flights were conducted during daytime except the one on May 24, which sampled during the late afternoon to nighttime transition period. Smaller N_2O signals were observed on this flight compared to the others because of trapping of emissions in the shallow nocturnal boundary layer, inaccessible to the plane.

[9] Real-time 1 Hz observations were aggregated based on observed spatial correlations to reduce the influence of atmospheric variability associated with turbulent eddies, which are not resolved in the transport model. The horizontal correlation length was determined to be ~8 km using exponential semivariogram analysis [*Gerbig et al*., 2003; *Kitanidis*, 1997], corresponding to roughly 0.05° in latitude and 0.06° in longitude within the Central Valley. The vertical correlation length was difficult to determine because of the limited number of vertical profiles and hour-of-day effects, and hence, this parameter was set to the size of large turbulent eddies

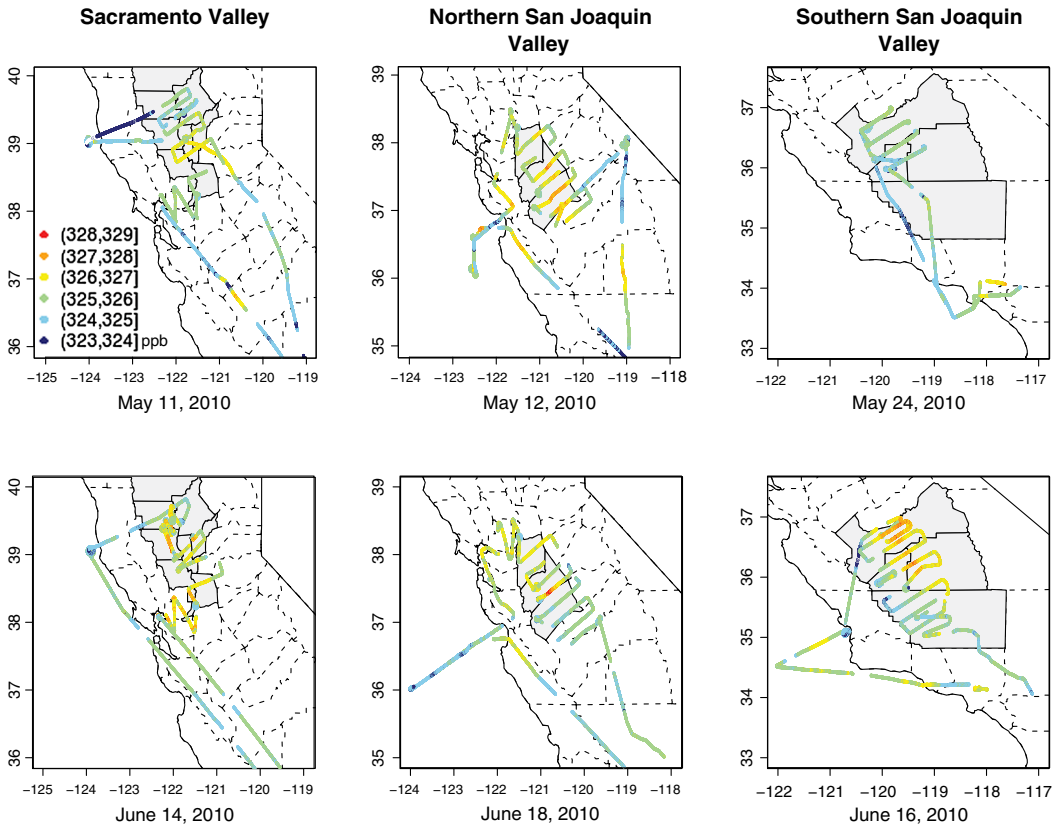

Figure 1. Central Valley N_2O profile. The bottom plots cover the same study areas (in gray) as the above ones, but a month later.

(around 200 m) observed within the boundary layer. We block-average data based on P-3 sampling locations and times within each grid defined by the horizontal and vertical correlation lengths. This aggregated dataset serves as the receptor points for comparison with model results.

3. Model Simulation

[10] We employed a top-down modeling approach coupled to a stepwise multiple linear regression (SMLR) to simulate the observed N_2O signals and estimate regional N_2O emissions. The method requires three essential inputs: (1) a meteorology field to drive a Lagrangian particle dispersion model (LPDM) that links observed atmospheric concentrations at the receptor points to upwind region surface emissions; (2) observation-based N_2O boundary conditions to provide the modeled background concentrations of air entering the Central Valley from the remote Pacific Ocean; and (3) spatial distributions and temporal changes of California's N_2O emission sources, to be coupled with the transport. A discussion of these three inputs and the statistical optimization methods used follows.

3.1. WRF-STILT LPDM Transport Model

[11] We coupled the weather research and forecasting meteorology to the stochastic time-inverted Lagrangian transport model (WRF-STILT) [*Lin et al.*, 2003; *Gerbig et al.*, 2003] in order to trace air parcels backward in time from our receptor points. The WRF model output used here was compiled specifically for CalNex by *Angevine et al.* [2012]. STILT uses the time-averaged horizontal and vertical wind fields to compute tracer mass fluxes, and planetary boundary layer heights (PBLH) to determine the surface influence for each time step along the particle trajectories. STILT represents the influence of turbulent motions using a Markov chain parameterized from the turbulent kinetic energy and Lagrangian time scales generated by WRF.

[12] We obtained results for STILT using two distinctly configured WRF outputs, GM4/GM12 and EM4N [*Angevine et al.*, 2012] (see Table 1), to test sensitivity of our results to WRF implementation. They differ primarily in the initial conditions and in the selection of land surface model. The GM4/GM12 runs (hereafter referred to as WRF 9) received initial meteorological fields from the U.S. National Centers for Environmental Prediction (NCEP) Global Forecast System

Table 1. Primary Configurations of Two WRF Runs Used in This Study[a]

Name	Initialization	PBL Scheme	Grid Spacing (km)	WRF Version	Vertical Levels	Land Surface Model, Data
GM4(WRF 9)	NCEP-GFS	MYJ	4	3.2.1	40	Slab, USGS
EM4N(WRF 23)	ECMWF-ERA	MYJ	4	3.3	60	Noah UCM MODIS

[a]This table is adapted from *Angevine et al.* [2012]. See text for more details and difference discussions.

(GFS) analyses, while the EM4N run (hereafter referred to as WRF 23) was initialized from the European Center for Medium-Range Weather Forecasts Interim Reanalysis (ERA-Interim). The latter initialization scheme has a deeper and moister boundary layer, especially over the ocean, compared to the former. WRF 9 employed the simple five-layer thermal diffusion land surface model ("slab") with U.S. Geological Survey (USGS) land use data. WRF 23 employed the Noah land surface model with newer MODIS land use/cover data and a single-layer urban canopy model (UCM). WRF 23 displayed smaller bias errors for PBLH compared to WRF 9, reflecting a PBL too cool, moist, and shallow in WRF 9. Other configuration settings such as WRF version, number of vertical levels, and one-way (WRF 9) or two-way (WRF 23) nesting did not make significant differences between the two WRF outputs. Both outputs modestly overestimated horizontal wind speeds.

[13] The WRF-STILT model simulates the N_2O concentration at a receptor point by adding the enhancements from surface emissions to the background concentration, at each STILT time step. The N_2O enhancement (in ppb) at the receptor location is obtained by summing the product of the footprint (in ppb/(μmol/m^2 s)) and surface flux (in μmol/(m^2 s)) at each grid cell. At the beginning of each receptor run, 500 particles were released from the receptor point at the same time and they traveled upwind, backward in time. The surface emissions were assumed to be well mixed within a volume ("mixed column"), set to be 50% of the PBL height from the WRF output (results are insensitive to the selection of 50% of PBLH for input of surface emissions) [see *Gerbig et al*., 2003]. Whenever released particles go below this height, the concentration of N_2O is increased to account for surface emissions in the corresponding grid cell. The influence from a particular upwind surface grid cell at the receptor point is quantified by tallying the total amount of time each particle spends in a finite volume over a time step [*Lin et al*., 2003]. We impose a N_2O boundary condition at the western edge of the meteorology model domain. STILT trajectories were run 10 days back in time to ensure that all 500 particles exited the WRF domain over the remote Pacific. Depending on the ending latitude and altitude, each particle was assigned a background concentration from the N_2O western boundary. The background concentration for each receptor point was the average value from all 500 released particles.

3.2. N_2O Remote Boundary

[14] Near surface sources, N_2O enhancements are usually ≤1% relative to the background concentrations. Negative excursions that may be associated with stratospheric air mixed down into the lower atmosphere are on the same order. In order for the model to capture these small changes and to accurately constrain surface fluxes, N_2O concentrations in the upwind remote boundary should be estimated with an accuracy of ~0.1 ppb.

[15] We use the NOAA Earth System Research Laboratory's North American lateral boundary condition data as the CalNex N_2O background. The background is the N_2O concentration in air traveling across the Pacific before reaching the North America continent. The NOAA dataset gives the time, latitude, and altitude variation of N_2O concentrations in the air entering North America from the remote Pacific. This boundary curtain is an empirical product derived from smoothed data obtained by aircraft and at Pacific Ocean sites, assuming that vertical gradients of N_2O with respect to marine boundary layer observations on average vary with season but are constant from year to year and can be extended through time by adding the annual increments. The receptor background concentrations derived from the NOAA boundary were systematically lower than the CalNex data in the free troposphere, reflecting small calibration biases. Therefore, we raised the NOAA boundary by the mean offset (1.6 ppb) to match free tropospheric observations above 2 km for each flight in CalNex, after filtering by STILT 10 day backward trajectories to ensure no surface influence. We also excluded periods of low N_2O air intrusions from the stratosphere by using CalNex O_3 observations [*Langford et al*., 2012].

3.3. Emission Inventories

[16] We assess four bottom-up emission estimates over California: (1) Emission Database for Global Atmospheric Research (EDGAR), version 3.2 Fast Track 2000 (hereafter referred to as EDGAR 2000); (2) EDGAR version 4.0 (hereafter referred to as EDGAR 4); (3) Global Emission Inventory Activity (GEIA); and (4) Dynamic Land Ecosystem Model (DLEM) [*Tian et al*., 2010].

[17] EDGAR 2000 and GEIA are global emission inventories with 1° × 1° spatial resolution. The EDGAR inventories cover all anthropogenic source categories of N_2O, including fossil fuel/biofuel/ industrial production, transformation and consumption, agricultural activities, biomass burning, and waste handling. EDGAR 4 is an updated version with spatial resolution of 0.1° × 0.1°. Global N_2O emissions from EDGAR 4 are 25% lower than those from EDGAR 2000, resulting largely from a change in the Intergovernmental Panel on Climate Change emission factor for direct soil sources (dropped from 0.0125 to 0.01 kg N_2O/kg N). The GEIA inventory includes both natural (such as soil and ocean emissions) and anthropogenic sources (such as agricultural waste burning, animal excreta, biofuel and fossil fuel burning, postforest clearing enhances, and industrial emissions). Previous studies using the top-down approach to constrain North American N_2O emission sources in early summer found the EDGAR 2000 emissions to be significantly too low, by almost a factor of 3 [*Kort et al*., 2008; *Kort et al*., 2010]. *Miller et al*. [2012] suggested monthly adjustments for the EDGAR and GEIA inventories based on the analysis of an ensemble of tall tower data over the central United States in 2008. The largest corrections for all three inventories appeared in the month of June, with the seasonal correction of nearly an order of magnitude in the case of EDGAR 4.

[18] The DLEM is a process-oriented biogeochemical model simulating land surface emissions of N_2O, among other species. DLEM couples major biogeochemical and hydrological cycles with vegetation dynamics and meteorological data to make daily estimates of carbon/nitrogen/water fluxes and pool sizes in terrestrial ecosystems [*Tian et al*., 2010]. The DLEM 2008 North America data have daily N_2O emission with 0.25° × 0.25° spatial resolution covering the entire United States.

3.4. Auxiliary Maps

[19] We found that the above emission inventories do not appear to provide good spatial representations of surface emissions as seen by the measurements (see section 4.2). We therefore employed a variety of land use and agricultural activity maps to provide independent information on the spatial patterns and source strengths of California N_2O emissions. The auxiliary maps include (1) California land use maps; (2) California dairy farm density, urban, highway, interstate, and airport maps; (3) California county-based livestock and crop data; (4) global cropland/pasture maps and fertilizer/manure application rate maps; and (5) California county-based fertilizer tonnage reports (data sources: California Department of Water Resources (CDWR); CalNex project website (http://www.esrl.noaa.gov/csd/calnex); National Agricultural Statistics Service; *Potter et al*., 2010; *Ramankutty and Foley* [1999]; and California Department of Food and Agriculture). The CDWR land use dataset partitions agricultural land into over 70 crop categories and land types including semi-agricultural, urban, native, and unclassified areas. Those categories (summarized in Table 2) cover in great detail the major terrestrial sources for N_2O, both natural and anthropogenic. Maps are available in geographic information system shapefiles with reported spatial resolution of 1 m and accuracy of 15 m.

[20] All auxiliary maps are gridded or regridded to $0.1^\circ \times 0.1^\circ$ resolution in order to couple with the STILT footprint maps. The gridded maps contain information on area coverage (e.g. CDWR maps), number density (e.g. number of cows), activity strength (e.g. fertilizer application rate), or index per grid cell (e.g. line sources such as highways and interstates) for each potential source. Gridding for point/line sources degrades their spatial resolution but still preserves the overall distribution pattern. One disadvantage of these maps is that there exist no associated emission factors or rate information. Hence, we derive emission rates for each of several selected major land categories for CalNex flight observations under the assumption that the emission rate is the same for individual source type throughout California at a given time. In reality, however, N_2O emissions may be heterogeneous and condition specific. Climatological factors, especially soil water content, can also influence soil emissions. Considering the particular time period and the location of this study, spatial variations in soil moisture will mostly reflect differences in irrigation (and hence the land use) more than variations in regional climate. Because of the aggregation provided by atmospheric transport and the wide areas that we sampled, our estimates of emission rates are expected to be representative of emissions associated with the land uses at the locations in California that contribute most to our observed atmospheric enhancements.

3.5. Statistical Optimization

[21] We used SMLR to assess the relationships between observed concentrations and sources of N_2O. In SMLR, the explanatory variables are the modeled contributions either from the subcategories of the EDGAR and GEIA emission inventories or from the modeled land source/human activity influences defined by the auxiliary spatial datasets. The observed values in SMLR are the N_2O enhancements, calculated by subtracting the modeled background from the flight observations. We select major source types in a forward stepwise way based on the Akaike's Information Criteria (AIC) [*Akaike*, 1974] and use nonnegative least squares to constrain the regression coefficients to be nonnegative [*Lawson and Hanson*, 1987]. Stepwise AIC for variable selection was shown mathematically to lead to the same method as partial F test [*Yamashita et al*., 2007]. The AIC statistics tests the significance of each variable and adds a penalty for the increasing number of variables in the model to prevent overfitting. Rates of soil uptake of N_2O are expected to be insignificant [*Syaklia and Kroeze*, 2011], so we do not allow negative variable contributions in the regression. This method is performed iteratively until all remaining predictors are considered insignificant (F limit < 4).

4. Results and Discussion

4.1. Transport Model Evaluation

[22] Constraints on source strength and associated uncertainties are sensitive to different aspects of the transport model, and these sensitivities must be considered on a case by case basis [*Nehrkorn et al*., 2010; *Lauvaux et al*., 2009]. We evaluated WRF-STILT model outputs by checking WRF PBLH against P-3 *in-situ* observations and by comparing STILT footprints derived from the two different WRF outputs. In this study, STILT uses the PBLH parameter directly from WRF to calculate footprints. We find the modeled WRF PBLH to be generally representative of the *in-situ* PBLH, which is determined from 90 vertical flight profiles during the daytime and over land by referencing to a suit of meteorological parameters and tracer gases measured on the P-3. Mean PBLH differences from the Central Valley flights (model - *in situ*) are -101.9 ± 262.1 m (1 standard deviation) for WRF 23 and -169.4 ± 341.7 m for WRF 9. This bias (-13% on average) may contribute to errors in the retrieved emission fluxes. But lacking a true ensemble of WRF-STILT models, one cannot give quantitative error bars for this. Some minor issues in WRF PBLH cannot be neglected, such as the nighttime and coastal low values, variability over small regions, and slightly different performance between the Los Angeles region and the Central Valley region. These issues all contribute to errors in simulation of

Table 2. California Land Use Classes and Subclasses from CDWR

Class	Subclass				
Agriculture	Grain and hay crops			Truck, nursery, and berry crops	
	Deciduous fruits and nuts			Citrus and subtropical	
	Rice	Field crops		Pasture	Vineyards
Semi-agriculture	Farmsteads, livestock feed lot operations, dairies and poultry farms				
Urban	Residential	Commercial	Industrial	Landscape	Vacant
Native	Vegetation			Riparian vegetation	
	Water surface			Barren and wasteland	

the transport model and are difficult to quantify. Horizontal and vertical winds are another important WRF input to STILT trajectory simulations. WRF outputs modestly overestimated horizontal wind speed [*Angevine et al.*, 2012], which may result in slightly low footprints around the receptor locations and extended footprint areas. The combined impacts of these meteorological variables on the transport model show up in the calculated footprint maps.

[23] We compare the footprint maps from WRF 9 and WRF 23 runs, and they show similar spatial patterns for the surface influences, with inferred sensitivity of WRF 23 footprints slightly larger within the Central Valley for most of the flights (Figure 2). The larger footprint from WRF 23 is in accordance with its deeper PBLH in the Central Valley [*Angevine et al.*, 2012]. We set STILT to output footprint maps at $0.1^\circ \times 0.1^\circ$ spatial resolution in order to distinguish land sources and to be coupled to EDGAR 4.

[24] The mean footprint maps revealed strong local influences from the Central Valley, which allow us to constrain agricultural area N_2O emissions of California. The resemblance in both magnitude and spatial pattern of the mean footprints from the two WRF runs builds our confidence in the reliability of the transport model results. Meanwhile, the modest discrepancies between the N_2O enhancements inferred from these two footprints allow a straightforward estimation of the meteorology-introduced uncertainties on our final results.

4.2. N_2O Emission Inventory Evaluation

[25] We evaluated the EDGAR 4, EDGAR 2000, GEIA, and DLEM inventories for California by coupling them to WRF-STILT and comparing modeled concentrations to observations during the Central Valley flights. All of the inventories indicate widespread N_2O emissions within the Central Valley and predict a very heterogeneous source distribution across the state (Figure 3). EDGAR 2000 and GEIA indicate strong urban emissions from the San Francisco Bay area and the South Coast Air Basin. With 100 times increased spatial resolution, EDGAR 4 appears to single out the northern part of the San Joaquin Valley, the Silicon Valley, and the costal part of the Los Angeles region among the strongest N_2O source regions, with emission rates as high as 1 nmol/(m^2 s). DLEM only simulates soil and agricultural sources and does not show industrial emissions in San Francisco and Los Angeles areas. It shows high emissions in the southern San Joaquin Valley, likely due to manure management of dairy farms that are concentrated in that area.

[26] Inventories that provide one value throughout the year (i.e. EDGAR and GEIA) all underestimate the California N_2O emissions that we observed in May and June. Figure 4 shows an example of the model data mismatch on the May 12th flight. The measurements (in black) exhibit surface N_2O enhancements on the order of 2 ppb and free tropospheric/mountain air as low as 325 ppb. The simulated N_2O signal concentrations (in orange) using the WRF 9 meteorology and the EDGAR 4 inventory are considerably low and poorly correlated with the observations, indicating both a mismatch of the spatial distribution of emissions and underestimation of the magnitudes. Similar results are found for EDGAR 4, EDGAR 2000, GEIA, and DLEM inventories for all six Central Valley flights.

[27] Source optimizations are conducted on the EDGAR 4 inventory subcategories using the SMLR method. We test the significance of contributions upon the subcategories and find that the agricultural management, road transportation, and livestock categories make the largest contribution to the observed N_2O enhancements (for both WRF 9 and

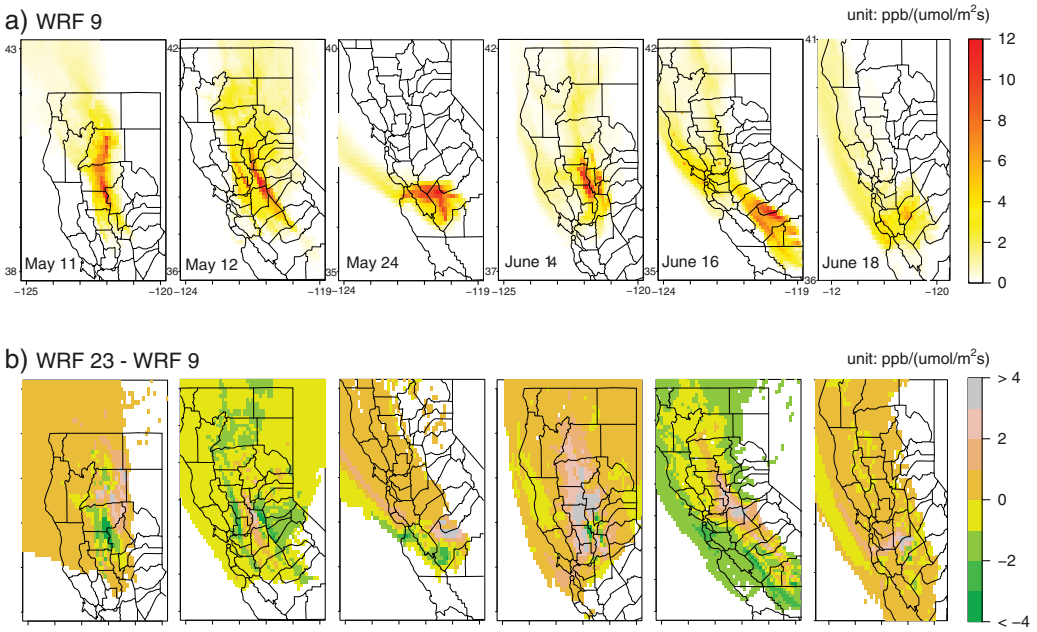

Figure 2. (a) Mean footprint maps averaged for all receptors for each Central Valley flight, calculated from WRF 9 coupled with STILT. (b) Mean footprint differences between WRF 23 and WRF 9. These WRF footprint differences, if coupled to the EDGAR 4 emission inventory, result in the mean differences of simulated N_2O for each flight of no more than 0.13 ppb.

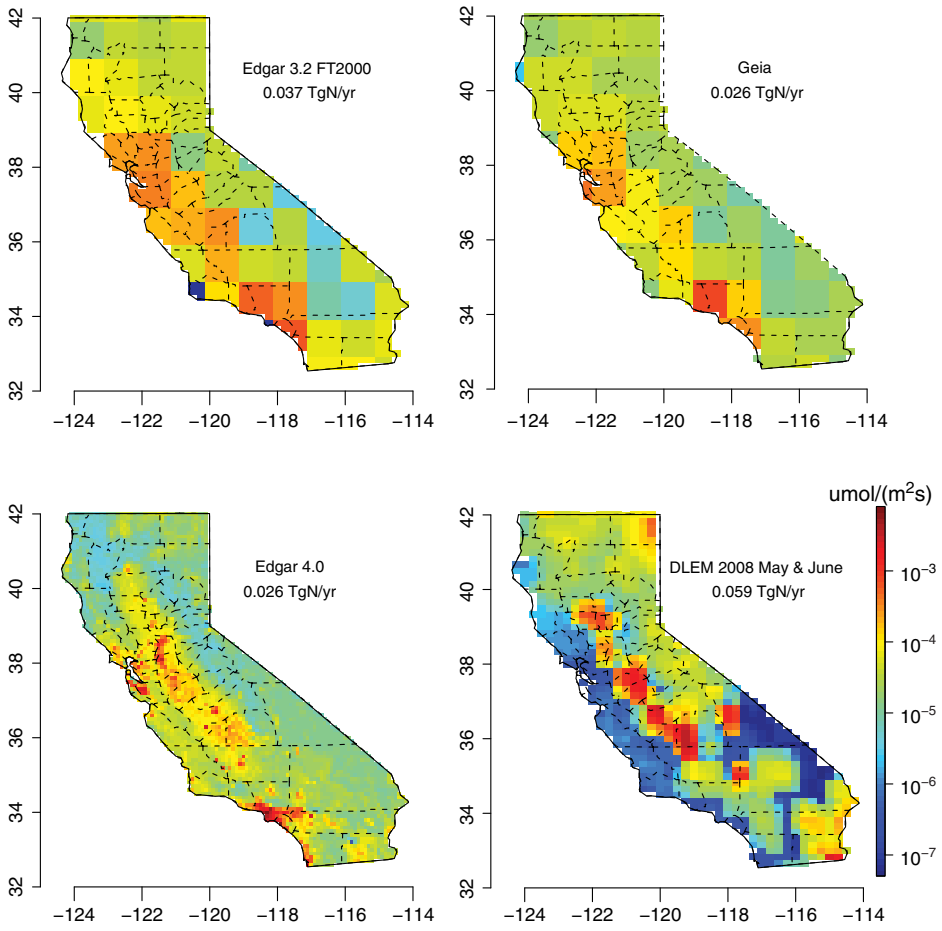

Figure 3. Emission inventory maps over California. DLEM map is the 2 month average of daily output for May and June in 2008.

WRF 23). The optimized results, however, still miss most of the high N_2O events in both time and magnitude. This indicates that EDGAR 4 underestimates emission strengths and has incorrect spatial distributions of sources in California. Conclusions for EDGAR 2000 and GEIA are similar: The poor correlations with the time series of observations are not markedly improved by the SMLR optimization of emissions categories, indicating likely erroneous representations of the spatial patterns in all of these inventories.

4.3. Model Optimization Using California Land Use and Activity Maps

[28] In order to improve the model representation of observations and to infer more accurate N_2O regional emissions from flight observations, we incorporate the auxiliary maps described above as predictor variables in our optimization statistics. California land use maps are coupled to footprint maps, and associated influences summed up to give the total influences of certain land use types at the receptors. Source types that contribute to the enhanced CalNex signals were selected using SMLR. The resulting regression coefficients represent the emission factors/rates for each land type. The regression intercept represents an estimate of the N_2O concentration enhancements transported over land from outside California, which may be compared to our boundary values. The scaled auxiliary spatial datasets sum to produce an estimated N_2O source map for California.

[29] Model data comparisons are improved by the use of auxiliary land use maps compared to emission inventories, as indicated by the red line in Figure 4. California land use maps of truck crop (noted as T in CDWR), rice (R), cows, native water (NW), and urban commercial (UC) are selected by the AIC as the top contributing sources to the flight observations. From Figure 4, the optimized model now captures the peak signal positions most of the time, with errors up to 25% in magnitude for some events. Besides the transport model error, this magnitude mismatch might also suggest nonuniform flux rates for the same land type or temporal variability in the sources. In particular, N_2O fluxes can spike rapidly after rainfall and fertilizer application [*Dobbie and Smith*, 2003]. This type of enhancement cannot be captured by the optimization because the data cannot constrain so many degrees of freedom. The model shown here explained 54% (R^2) of the observed variance, with the residual attributed to undefined temporal events and uncontrolled factors, such as environmentally sensitive emission rates and meteorological uncertainties.

[30] The categorical contributions to N_2O signals are shown in the lower plot of Figure 4. The crop category (T + R) provides the most variability and contributes up to 1.4 ppb N_2O to the measured signals, suggesting that fertilizer application

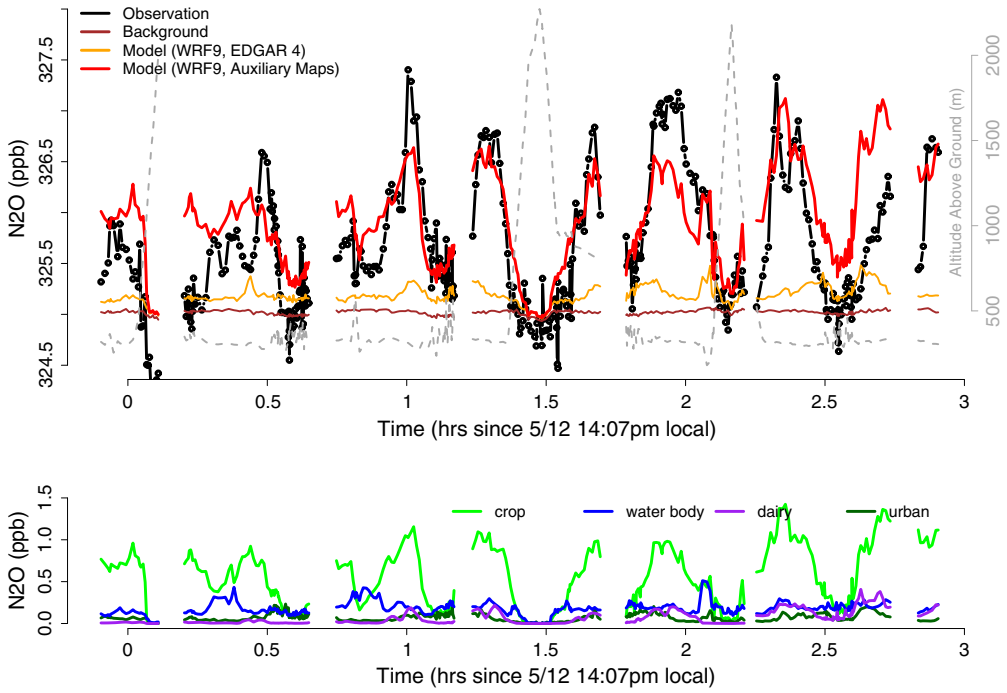

Figure 4. Modeled N_2O signals for Northern San Joaquin Valley flight on May 12, 2010 (see flight track in Figure 1). Upper plot: Time series plot of observation (black), modeled background (brown), modeled results using EDGAR 4 (orange), and optimization results using auxiliary maps (red). Data gaps are due to in-flight calibrations. Lower plot: Major land use–based source contributions to N_2O signal derived from optimization.

and agricultural management are the biggest N_2O source in the Northern San Joaquin Valley. The general emissions rate for crops is 0.02 μmol/(m^2 s), which is within the literature reported range of 10^{-4} and 0.12 μmol/(m^2 s) [*Yanai et al.*, 2003; *Turner et al.*, 2008]. The second contributing source is native water (NW), resulting from leaching and runoff of fertilizers, as well as aquatic microbial processes [*Seitzinger and Kroeze*, 1998, and references therein]. Crop and native water categories together contributed over 80% of the simulated N_2O signal. We checked our model performance (the coupled surface fluxes and WRF-STILT) on the regional scale by plotting vertical profiles of N_2O for a total of three P-3 flight profiles in the Northern San Joaquin Valley (Figure 5); these data were not used in the SMLR. The good agreement of the model vertical gradient with observations demonstrates the overall ability of the model and the source optimization framework. The model over the Walnut Grove Tower captures the vertical distribution very well, though with a positive bias. This is likely a boundary condition issue, where the adjusted NOAA boundary misrepresents the upwind N_2O concentrations of the corresponding receptors.

4.4. California N_2O Emissions

4.4.1. Major Sources

[31] Major N_2O emission sources in California are dominated by fertilizer application, leaching, and runoff, inferred from CalNex Central Valley flight observations. We conducted the same SMLR statistical optimizations for each of the six agricultural flights and also for combined flight observations using the two WRF meteorological fields. The resulting major land use categories and the associated model data correlation coefficients are summarized in Table 3. Our optimized results for each flight are very similar for the two WRF models. Poor model representations for a few flights can be attributed to meteorological model errors, for example, the case of low nighttime PBLH from WRF for May 24th flight or low coastal PBLH for the June 18th flight.

[32] There may be additional important transient N_2O emissions that we do not account for explicitly, such as the flooding of rice field and the coastal ocean upwelling. Missing short-term emission sources could be the reason for poor model optimization results for June 14 and 18. The June 14th flight was a revisit to the rice fields in the Sacramento Valley, and significant N_2O enhancements were observed from this flight compared to the May 11th flight (see Figure 1). MODIS satellite images reveal extensive flooding in this area at the end of May, and rice planting and growth afterward in June [*Peischl et al.*, 2012]. The enhanced N_2O signals seen by the P-3 might be attributed to stimulation of nitrogen cycle processes by inundation and fertilizer application during rice planting. This possibility is supported by the simultaneously observed CH_4 enhancement observed by QCLS-DUAL on the P-3, which is coemitted from the flooded rice fields [*Cai et al.*, 1997; *Khalil et al.*, 1998]. Coastal ocean upwelling of N_2O-rich water can also be a significant source to the June 18th flight measurements (see Figure 2) and possibly to the overall atmospheric boundary. *Nevison et al.* [2004] suggested that coastal upwelling could contribute up to 2 ppb N_2O, comparable to the values we observed in CalNex during some coastal flights. We tested this effect by including the California coastal area (within 100 km offshore) as a land use category in the SMLR analysis. Results show that coastal ocean upwelling could explain

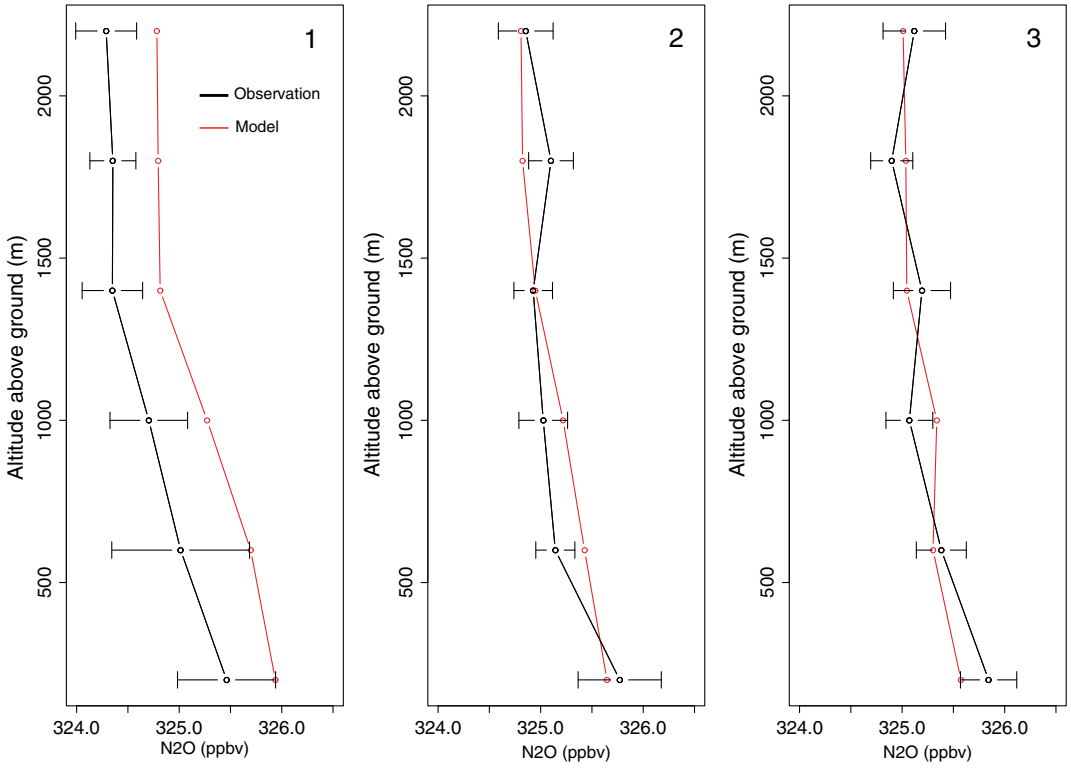

Figure 5. Vertical profiles of observed and modeled N_2O over (1) Walnut Grove Tower (38.3°N, 121.5°W), (2) corn field (37.3°N, 121.0°W), and (3) San Luis Reservoir (37.1°N, 121.1°W). Observations are averaged within 400 m bins.

Table 3. Land Use/Cover Categories Identified as Significant N_2O Sources to CalNex Agricultural Flight Observations, Derived from Two WRF Outputs

Flight	Meteorology (WRF)	Land Use/Cover	R^2 [b]	R^2 (Single Scaling)	
				EDGAR4	GEIA
May 11 Sacramento Valley	9	fertilizer[a], G, V, UC, C	0.43	0.003	0.02
	23	fertilizer, NR, V, UR	0.49	0.02	0.01
May 12 Northern San Joaquin Valley	9	T, R, cow, NW, UC	0.54	0.14	0.07
	23	T, R, cow, NW, interstates	0.53	0.19	0.11
May 24 Southern San Joaquin Valley	9	NW, interstates	0.16	0.008	0.07
	23	R, S	0.10	0.003	0.005
June 14 Sacramento Valley	9	NR, UL, NW, R, G, V	0.36	0.16	0.06
	23	F, NR, UI7	0.26	0.06	0.07
June 16 Southern San Joaquin Valley	9	V, UR, cow, UL, C	0.57	0.28	0.26
	23	V, UR	0.57	0.39	0.33
June 18 Northern San Joaquin Valley	9	urban, ocean upwelling	0.26	0.21	0.26
	23	urban, ocean upwelling	0.25	0.22	0.26
May Flights(5/11, 12, and 24)	9	R, G, cow, manure, interstates	0.31	0.17	0.15
	23	T, R, cow, interstates	0.38	0.12	0.13
June Flights(6/14, 16, and 18)	9	V, R, cow, urban, UL, C	0.34	0.13	0.10
	23	V, NV, railroads	0.29	0.23	0.19
All Flights(5/11, 12, 24, and 6/14, 16, 18)	9	UL, cow, R, C, V, interstates	0.33	0.16	0.10
	23	cow, NW, interstates, UL, R	0.29	0.25	0.22

[a]Fertilizer, global fertilizer application map [*Potter et al.*, 2010]; G, grain and hay crops (CDWR); V, vineyards (CDWR); UC, urban commercial (CDWR); C, citrus and subtropical (CDWR); NR, native riparian vegetation (CDWR); UR, urban residential (CDWR); T, truck, nursery and berry crops (CDWR); R, rice (CDWR); cow, California cow map (CalNex website); NW, native water surface (CDWR); interstates, California interstates map (CalNex website); S, semi-agricultural and incidental to agriculture (CDWR); UL, urban landscape (CDWR); F, field crops (CDWR); UI7, the oil refineries subcategory of urban industrial (CDWR); urban: California urban map (CalNex website).
[b]All correlations in this column are significant with $P << 0.001$.

on average 0.2 ppb (WRF 9) and 0.3 ppb (WRF 23) of the observed N_2O signal on June 18, but the effect was relatively small overall.

4.4.2. Emission Maps and Statewide Total Emissions

[33] We estimated California N_2O emission maps for the months of May and June separately, derived from the CalNex

airborne observations. We choose flights with better model representation of the observations in each month, which are on May 12 and June 16 (Table 3), to construct these maps. The selected land use maps (first multiplied with the derived coefficients) are summed up at each grid cell to give the total flux map. For each flight, we plotted the optimized mean flux map from WRF 9 and WRF 23 outputs within the influential areas, shown in Figure 6. These constructed maps are compared to EDGAR 4, which has the highest spatial resolution among current N_2O inventories, and the differences are also plotted in Figure 6.

[34] The N_2O flux maps from this study show quite different spatial patterns versus the EDGAR 4 inventory and also show variation between the May and June flight dates. The modeled maps capture spatially extensive sources from the Central Valley, as well as grid cell scale sources near the mountains in the north. The model indicates concentrated high emissions in the Northern San Joaquin Valley in mid-May, which are absent in June. The Sacramento Valley and the Southern San Joaquin Valley have more sporadically distributed sources in mid-June. This suggests that the peak crop N_2O emissions in California are in May, earlier than the Great Plains and the Midwest agricultural area [*Miller et al.*, 2012], as might be expected from the longer-growing season in California. The concentrated N_2O sources in the northern Central Valley from the May 12th model have emission rates over 4 nmol/(m^2 s) higher than those from EDGAR 4. The modeled June 16th map shows that the northern Central Valley has passed its growing peak but still maintains broad emissions at around 1 nmol/(m^2 s), close to the EDGAR 4 values. This emission transition feature does not show up in EDGAR or GEIA because of the lack of seasonality in these inventories.

[35] If we assume the same source contributions and apply these optimization results from the flight footprint areas to all of California, statewide N_2O emissions in May (based on all three May flights) would be 0.0096 Tg N using WRF 23 and 0.0110 Tg N using WRF 9, and in June (based on all three June flights) would be 0.0060 Tg N using WRF 23 and 0.0059 Tg N using WRF 9. The 95% confidence intervals for these budget estimations are (0.0086, 0.0106), (0.0092, 0.0127), (0.0052, 0.0068), and (0.0053, 0.0065) Tg N, respectively, obtained from bootstrapping the linear regressions under each case. The uncertainties from meteorology (up to 22% based on WRF 23 and 9 comparisons) and from the statistics (up to 15% based on bootstrap results) together contribute ~27% errors to the estimated emissions, which are modest compared to the increase between EDGAR 4 and our optimized results in May and June. To estimate the annual budget, we extrapolate the derived

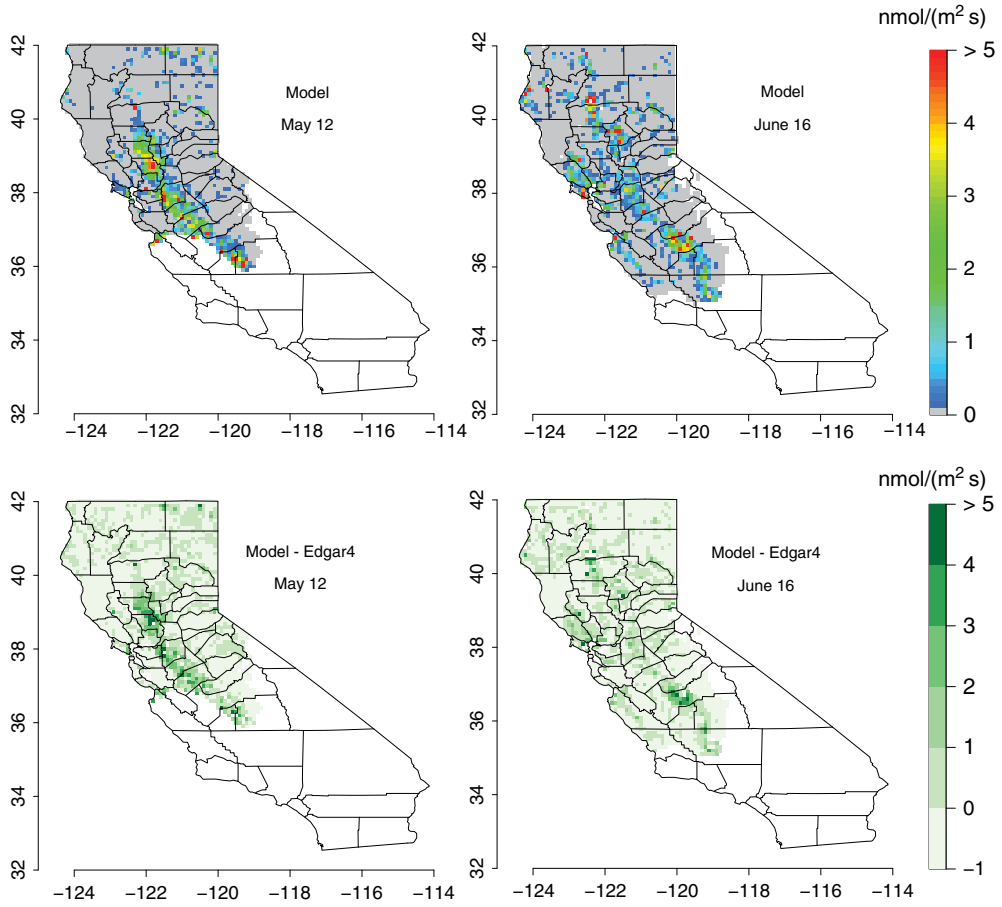

Figure 6. California N_2O emissions maps, inferred from May 12th flight and June 16th flight. Upper plots: Model-derived flux maps (absolute scale) within the footprint area. White areas had no influences on the aircraft observations; they do not mean zero surface fluxes. Values less than 0.1 nmol/(m^2 s) are displayed in gray. Lower plots: N_2O flux difference maps between model and EDGAR 4 within the footprint area.

Table 4. California Total Annual N_2O Emissions from Emission Inventories and This Study (Tg N/year)

Emission Inventory						
EDGAR 2000	EDGAR 4	GEIA	California 2009 GHG Inventory	DLEM	DNDC	This Study
0.037	0.026	0.026	0.032	0.059[a]	0.013[b]	0.042 ± 0.011

[a]This value is from DLEM outputs in 2008.
[b]The denitrification-decomposition model (DNDC) simulates microbe-driven soil emission of N_2O through processes such as decomposition, fermentation, nitrification, and denitrification [*Li et al*., 2000]. The value is from *Guo et al*. [2011].

May and June emissions by using the seasonal variations of N_2O emissions observed in the midwest United States [*Miller et al*., 2012] as a rough approximation to those in California, since we do not have observations covering the rest of the year. The average emissions in May and June are 2.3 times as high as the annual mean in that study. Our derived 2 month statewide budget is then scaled to an annual emission of 0.042 ± 0.011 Tg N, larger than the total given by EDGAR 2000, EDGAR 4, GEIA, and the California 2009 GHG emission inventories by factors of 1.14, 1.62, 1.62, and 1.31, respectively. This value is about 30% lower than the total for DLEM (Table 4). Note that the underlying spatial distributions in EDGAR, GEIA, and DLEM appear to be significantly in error for May and June, and the real spatial patterns may be expected to vary by season. Our estimated total emission values could be better constrained by conducting observations over multiple seasons and by better characterizing urban emission sources from CalNex urban flight analysis.

5. Conclusions

[36] This study provides high-resolution top-down N_2O source constraints for California. We find that existing regional and global N_2O inventories underestimate terrestrial fluxes and predict incorrect spatial distributions during the crop-growing season. We present a top-down estimate of emissions by optimizing our model data framework using land use maps and activity categories to provide an adaptive spatial representation of sources with low dimensionality. Our results suggest strong seasonal variations of total emission flux for N_2O in California during the peak agricultural growing season, with fluxes 3–4 times larger than the seasonally invariant values given by EDGAR and other inventories. The extrapolated annual California N_2O emission is 0.042 ± 0.011 Tg N, roughly 1–2 times the annual totals given by EDGAR, GEIA, and the California 2009 GHG Emission Inventory. To further characterize the seasonality and the strength of the California N_2O sources, long-term monitoring of N_2O concentrations is needed with greater spatial coverage. Our study supports the view that agricultural activities provide large sources of N_2O in California and that future N_2O mitigation strategies in California should focus on this sector.

[37] **Acknowledgments.** This study was supported by the following grants to Harvard University: NASA NNX09AJ94G, NNX11AG47G, and NNX09AU40G; NSF ATM-083091-2; and NOAA NA09OAR4310122 and NA11OAR4310158. We are grateful to the flight crew of the NOAA P-3 for safely executing a difficult flight mission. B.X. thanks Jasna Pittman for helpful comments on the manuscript. E.A.K. thanks the W. M. Keck Institute for Space Studies for support. Portions of this work were performed at the Jet Propulsion Laboratory, California Institute of Technology, under contract with NASA.

References

Akaike, H. (1974), A new look at statistical-model identification, *IEEE Trans. Autom. Control*, *6*, 716–723.

Angevine, W. M., L. Eddington, K. Durkee, C. Fairall, L. Bianco, and J. Brioude (2012), Meteorological model evaluation for CalNex 2010, *Monthly Weather Rev.*, *140*, 3885–3906, doi:10.1175/MWR-D-12-00042.1.

Cai, Z. C., G. X. Xing, X. Y. Yan, H. Xu, H. Tsuruta, K. Yagi, and K. Minami (1997), Methane and nitrouse oxide emissions from rice paddy fields as affected by nitrogen fertilizers and water management, *Plant Soil*, *196*, 7–14, doi:10.1023/A:1004263405020.

Crutzen, P. J., A. R. Mosier, K. A. Smith, and W. Winiwarter (2007), N_2O release from agro-biofuel production negates global warming reduction by replacing fossil fuels, *Atmos. Chem. Phys. Discuss.*, *7*, 11,191–11,205.

Davidson, E. A. (2009), The contribution of manure and fertilizer nitrogen to atmospheric nitrous oxide since 1860, *Nat. Geosci.*, *2*, 659–662.

Denman, K., et al. (2007), Couplings between changes in the climate system and biogeochemistry, in *Climate Change 2007*: *The Physical Science Basis*. *Contribution of Working Group I to the Fourth Assessment Report of the Intergovernmental Panel on Climate Change*, edited by S. Solomon et al., pp. 499– 587, Cambridge Univ. Press, Cambridge, U. K.

Dobbie, K. E., and K. A. Smith (2003), Nitrous oxide emission factors for agricultural soils in Great Britain: The impact of soil water-filled pore space and other controlling variables, *Global Change Biol.*, *9*, 204–218, doi:10.1046/j.1365-2486.2003.00563.x.

Gerbig, C., J. C. Lin, S. C. Wofsy, B. C. Daube, A. E. Andrews, B. B. Stephens, P. S. Bakwin, and C. A. Grainger (2003), Toward constraining regional-scale fluxes of CO2 with atmospheric observations over a continent: 1. Observed spatial variability from airborne platforms, *J. Geophys. Res.*, *108*(D24), 4756, doi:10.1029/2002JD003018.

Guo, L., D. Luo, C. Li, and M. FitzGibbon (2011), Development of spatial inventory of nitrous oxide emissions from agricultural land uses in California using biogeochemical modeling, *ACS Symposium Series*, vol. *1072*, chap. 20, pp. 387–403.

Jeong, S., C. Zhao, A. E. Andrews, E. J. Dlugokencky, C. Sweeeney, L. Bianco, J. M. Wilczak, and M. L. Fischer (2012), Seasonal variations in N_2O emissions from central California, *Geophys. Res. Lett.*, *39*, L16805, doi:10.1029/2012GL052307.

Jimenez, R., S. Herndon, J. H. Shorter, D. D. Nelson, J. B. McManus, and M. S. Zahniser (2005), Atmospheric trace gas measurements using a dual quantum-cascade laser mid-infrared absorption spectrometer, *Proc. SPIE*, *5738*, 318–331.

Khalil, M. A. K., R. A. Rasmussen, M. J. Shearer, Z.-L. Chen, Y. Heng, and J. Yang (1998), Emissions of methane, nitrous oxide, and other trace gases from rice fields in China, *J. Geophys. Res.*, *103*(D19), 25,241–25,250.

Kitanidis, P. K. (1997), Introduction to Geostatistics: Applications in Hydrogeology. Cambridge Univ. Press, Cambridge, U. K.

Kort, E. A., J. Eluszkiewicz, B. B. Stephens, J. B. Miller, C. Gerbig, T. Nehrkorn, B. C. Daube, J. O. Kaplan, S. Houweling, and S. C. Wofsy (2008), Emissions of CH_4 and N_2O over the United States and Canada based on a receptor-oriented modeling framework and COBRA-NA atmospheric observations, *Geophys. Res. Lett.*, *35*, doi:10.1029/2008GL034031.

Kort, E. A., *et al*., (2010), Atmospheric constraints on 2004 emissions of methane and nitrous oxide in North America from atmospheric measurements and a receptor-oriented modeling framework, *J. Integr. Environ. Sci.*, *7*(2), 125–133, doi:10.1080/19438151003767483.

Kort, E. A., P. K. Patra, K. Ishijima, B. C. Daube, R. Jiménez, J. Elkins, D. Hurst, F. L. Moore, C. Sweeney, and S. C. Wofsy (2011), Tropospheric distribution and variability of N_2O: Evidence for strong tropical emissions, *Geophy. Res. Lett.*, *38*, L15806, doi:10.1029/2011GL047612.

Langford, A. O., J. Brioude, O. R. Cooper, C. J. Senff, R. J. Alvarez, R. M. Hardesty, B. J. Johnson, and S. J. Oltmans (2012), Stratospheric influence on surface ozone in the Los Angeles area during late spring and early summer of 2010, *J. Geophys. Res.*, *117*, doi:10.1029/2011JD016766.

Lauvaux, T., O. Pannekoucke, C. Sarrat, F. Chevallier, P. Clais, J. Noilhan, and P. J. Rayner (2009), Structure of the transport uncertainty in mesoscale inversions of CO_2 sources and sinks using ensemble model simulations, *Biogeosciences*, *6*, 1089–1102.

Lawson, C. L. and R. J. Hanson (1987), Solving Least Squares Problems, Prentice-Hall, Englewood Cliffs, New Jersey.

Li, C. S., J. Aber, F. Stange, K. Butterbach-Bahl, and H. Papen (2000), A process-oriented model of N_2O and NO emissions from forest soils: 1. Model development, *J. Geophys. Res.*, *105*, 4369–4384, doi:10.1029/1999JD900949.

Lin, J. C., C. Gerbig, S. C. Wofsy, A. E. Andrews, B. C. Daube, K. J. Davis, and C. A. Grainger (2003), A near-field tool for simulating the upstream influence of atmospheric observations: The stochastic time-inverted Lagrangian transport (STILT) model, *J. Geophys. Res.*, *108*(D16), 4493, doi:10.1029/2002JD003161.

Miller, S. M., *et al*.,(2012), Regional sources of nitrous oxide over the United States: Seasonal variation and spatial distribution, *J. Geophys. Res.*, *117*, D06310, doi:10.1029/2011JD016951.

Montzka, S. A., E. J. Dlugokencky, and J. H. Butler, (2011), Non-CO_2 greenhouse gases and climate change, *Nature*, *476*, 43–50.

Nehrkorn, T., J. Eluszkiewicz, S. C. Wofsy, J. C. Lin, C. Gerbig, M. Longo, and S. Freitas (2010), Coupled weather research and forecasting–stochastic time-inverted Lagrangian transport (WRF–STILT) model, *Meteorol. Atmos. Phys.*, *107*, 51–64, doi:10.1007/s00703-010-0068-x.

Nevison, C. D., T. J. Lueker, and R. F. Weiss (2004), Quantifying the nitrous oxide source from coastal upwelling, *Global Biogeochem. Cycles*, *18*, GB1018, doi:10.1029/2003GB002110.

Peischl, J., *et al*.,(2012), Airborne observations of methane emissions from rice cultivation in the Sacramento Valley of California, *117*(D24), doi:10.1029/2012JD017994.

Potter, P., N. Ramankutty, E. M. Bennett, and S. D. Donner (2010), Characterizing the spatial patterns of global fertilizer application and manure production, *Earth Interact.*, *14*, 2, doi:10.1175/2009EI288.1.

Ramankutty, N., and J. A. Foley (1999), Estimating historical changes in global land cover: Croplands from 1700 to 1992, *Global Biogeochem. Cycles*, *13*, 997–1027, doi:10.1029/1999GB900046.

Ravishankara, A. R., J. S. Daniel, and R. W. Portmann (2009), Nitrous oxide: The dominant ozone-depleting substance emitted in the 21st century, *Science*, *326*, 123–125.

Seitzinger, S. P., and C. Kroeze (1998), Global distribution of nitrous oxide production and N inputs in freshwater and coastal marine ecosystems, *Global Biogeochem. Cycles*, *12*, 93–113, doi:10.1029/97GB03657.

Syakila, A., and C. Kroeze (2011), The global nitrous oxide budget revisited, *Greenhouse Gas Measurement and Manage.*, *1*, 17–26, doi:10.3763/ghgmm.2010.0007.

Szukics, U., G. C. J. Abell, V. Hodl, B. Mitter, A. Sessitsch, E. Hackl, and S. Zechmeister-Boltenstern (2010), Nitrifiers and denitrifiers respond rapidly to changed moisture and increasing temperature in a pristine forest soil, *FEMS Microbiol. Ecol.*, *72*, 395–406.

Tian, H., X. Xu, M. Liu, W. Ren, C. Zhang, G. Chen, and C. Lu (2010), Spatial and temporal patterns of CH_4 and N_2O fluxes in terrestrial ecosystems of North America during 1979-2008: Application of a global biogeochemistry model, *Biogeosciences*, *7*, 2673–2694, doi:10.5194/bg-7-2673-2010.

Turner, D. A., D. Chen, I. E. Galbally, R. Leuning, R. B. Edis, Y. Li, K. Kelly, and F. Phillips (2008), Spatial variability of nitrous oxide emissions from an Australian irrigated dairy pasture, *Plant Soil*, *309*, 77–88, doi:10.1007/s11104-008-9639-8.

Volk, C. M., J. W. Elkins, D. W. Fahey, G. S. Dutton, J. M. Gilligan, M. Loewenstein, J. R. Podolske, K. R. Chan, and M. R. Gunson, (1997), Evaluation of source gas lifetimes from stratospheric observations, *J. Geophys. Res.*, *102*, 25,543–25,564, doi:10.1029/97JD02215.

Wunch, D., P. O. Wennberg, G. C. Toon, G. Keppel-Aleks, and Y. G. Yavin (2009), Emissions of greenhouse gases from a North American megacity, *Geophys. Res. Lett.*, *36*, L15810, doi:10.1029/2009GL039825.

Yamashita, T., K. Yamashita, and R. Kaminura (2007), A stepwise AIC method for variable selection in linear regression, *Commun. Stat. Theory Methods*, *36*(13), 2395–2403.

Yanai, J., T. Sawamoto, T. Oe, K. Kusa, K. Yamakawa, K. Sakamoto, T. Naganawa, K. Inubushi, R. Hatano, and T. Kosaki (2003), Spatial variability of nitrous oxide emissions and their soil-related determining factors in an agricultural field, *J. Environ. Qual.*, *32*, 1965–1977.